ADVANCED HEALTHCARE MATERIALS
www.advhealthmat.de

Human Oral Motion-Powered Smart Dental Implant (SDI) for In Situ Ambulatory Photo-biomodulation Therapy

Moonchul Park, Sayemul Islam, Hye-Eun Kim, Jonathan Korostoff, Markus B. Blatz, Geelsu Hwang, and Albert Kim**

Peri-implant disease is an inflammatory condition affecting the soft and hard tissues surrounding a dental implant. However, current preventative methods are insufficient due to the limited bioactivity on the dental implant and poor patient compliance. Recently, photo-biomodulation (PBM) therapy that can recover and regenerate peri-implant soft tissue has attracted considerable attention in dentistry. In this paper, a seamless human oral motion-powered dental implant system (called Smart Dental Implant or SDI) is presented as an ambulatory PBM therapy modality. SDI allows the in situ light delivery, which is enabled by the energy harvesting from dynamic human oral motions (chewing and brushing) via an engineered piezoelectric dental crown, an associated circuit, and micro light emitting diodes (LEDs). The SDI also offers adequate mechanical strength as the clinical standards. Using primary human gingival keratinocytes (HGKs) as a model host organism and *Pseudomonas aeruginosa* lipopolysaccharides (LPS) as a model inflammatory stimulus, effective SDI-mediated PBM therapy is demonstrated. A new class of dental implants could be an ambulatory PBM therapy platform for the prevention of peri-implant disease without patient dependency, warranting long-lasting dental implants.

1. Introduction

Approximately 3 million Americans have at least one dental implant, and this number is propelling by the prevalence of tooth decay in the growing geriatric population as well as periodontal disease in the overall population.[1] The dental implant is the only restorative tooth replacement method that can preserve and stimulate natural bone growth. Oral rehabilitation with dental implants also helps in restoring oral function and facial form of a patient.[2,3] Although dental implants have become a reliable and routine component of the daily dental practice, failures do occur, resulting in discomfort, painful and costly surgeries, and the potential breakdown of overall oral health.[4–6] Especially, smokers and patients with a history of chronic periodontitis or diabetes are more vulnerable to early failures.[7–9]

The dental implant failure is primarily attributed to the susceptibility of the implant and implant-supported restorative surface to bacterial colonization (dental plaque) and the subsequent inflammation of gingival (gum) tissue (peri-implant disease) (**Figure 1**a).[10,11] Under the healthy oral condition, periodontal tissues protect the dental implant's surroundings against bacterial invasion. However, the peri-implant interface (junctional epithelium or tissue adjacent to the implant abutment) has been shown to be less effective than natural teeth in resisting bacterial invasion. Abnormal gingival fiber alignment and reduced vascular supply at the interface make the peri-implant tissue more vulnerable to subsequent peri-implant disease, resulting in the potent implant loss.[12,13] Additionally, current dental materials exhibit limited bioactivity to prevent peri-implant disease, and current treatment, such as plaque control or routine mechanical instrumentation, are insufficient due to poor patient compliance.[14–16]

There were many attempts to achieve the effective prevention of peri-implant disease by incorporating antimicrobial molecules in the restorative dental crown to reduce bacterial activity.[17,18] However, gradual passive losses of bioactive elements from the surface into the surrounding environment have limited its adoption to the clinic. Thus, a proactive approach that can efficiently recover and regenerate the host peri-implant soft tissue against bacterial intrusion is warranted. Among many tissue regenerative therapies, photo-biomodulation (PBM)

M. Park, S. Islam, Prof. A. Kim
Department of Electrical and Computer Engineering
Temple University
Philadelphia, PA 19122, USA
E-mail: albertkim@temple.edu
Dr. H.-E. Kim, Prof. M. B. Blatz, Prof. G. Hwang
Department of Preventive and Restorative Sciences
School of Dental Medicine
University of Pennsylvania
Philadelphia, PA 19104, USA
E-mail: geelsuh@upenn.edu
Prof. J. Korostoff
Department of Periodontics
School of Dental Medicine
University of Pennsylvania
Philadelphia, PA 19104, USA
Prof. G. Hwang
Center for Innovation & Precision Dentistry
School of Dental Medicine
School of Engineering and Applied Sciences
University of Pennsylvania
Philadelphia, PA 19104, USA

DOI: 10.1002/adhm.202000658

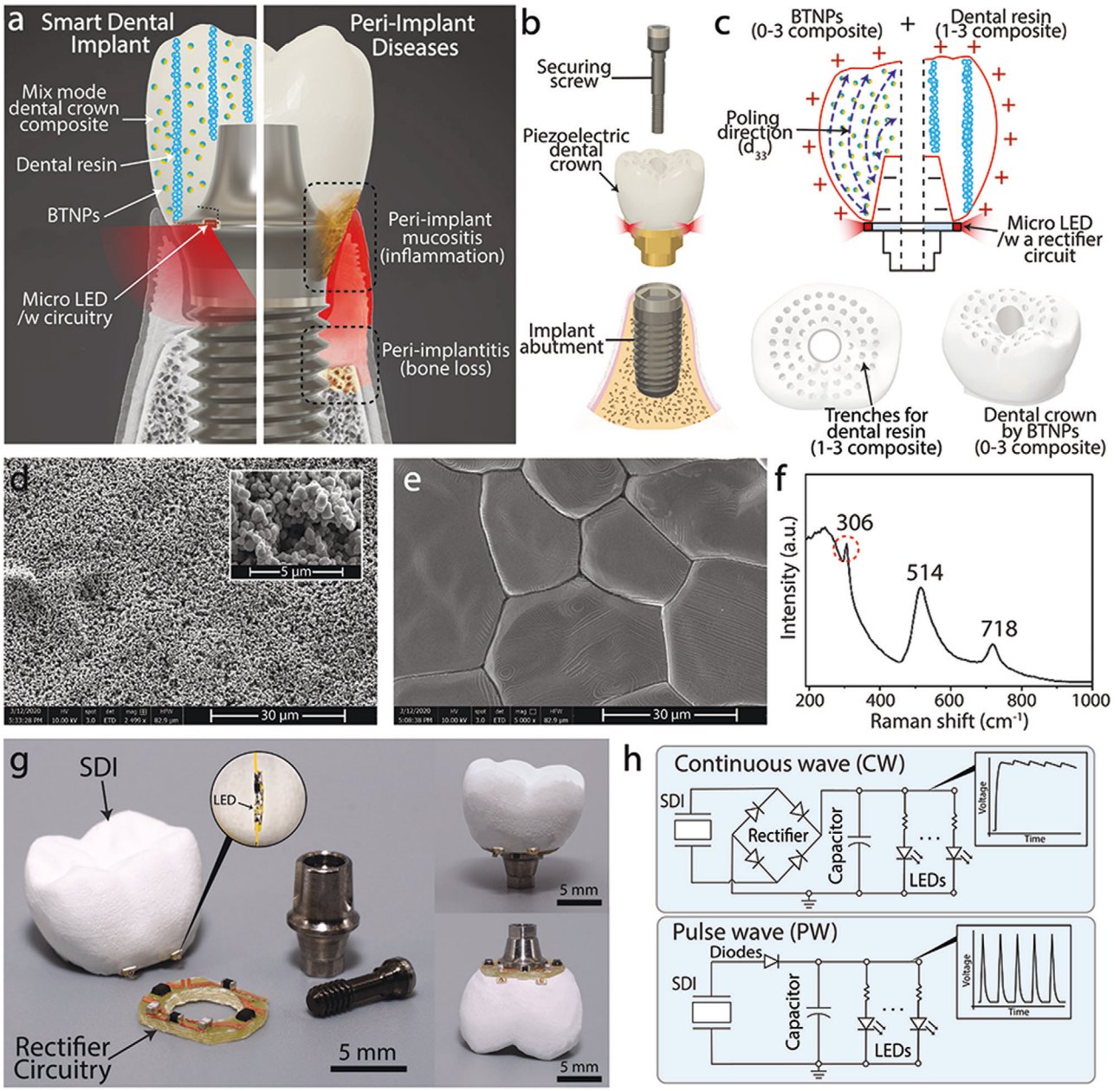

Figure 1. Illustration of Smart Dental Implant (SDI) system: a) ambulatory photo-biomodulation therapy enabled by SDI maintain overall oral health, while normal dental implant without therapeutic function can cause severe oral diseases (image was modified from the source: http://www.deardoctor.com/articles/peri-implantitis-can-cause-implant-failure/). b) Schematic view of SDI assembly based on a screw-retain dental implant design, consists of c) two-phase composite dental crown, associated electronics, and micro LEDs. d,e) SEM images of the engineered dental material: sintering process creates a bulk piezoelectric material (scales are 30 μm for both). The SEM working distance was 9.64 μm for (d) and 9.77 μm for (e), respectively. The magnification was 2500× for (d) and 5000× for (e). The field height × width was 82.9 × 55.3 μm with a resolution of (1536 × 1024 pixel^2). f) Raman characterization of BTNPs indicates the engineered dental material is indeed piezoelectric: a sharp peak at 306 cm^{-1} is the signature of the tetragonal lattice i.e., piezoelectricity. g) prototype SDI on a US penny. g) Converted PW using an integrated circuit. h) Two different types of integrated circuits for continuous wave (CW) or pulsed wave (PW).

therapy (also known as low-level light therapy (LLLT)) has been highlighted due to its significant biological effects.[19,20] Despite potent biological functions of photo-stimulation on promoting tissue healing, reducing inflammation, and attenuating bacterial activity, its adoption to dental care as an implantable mean has yet to exist due to the lack of reliable light delivering methods.

Here, we present a smart dental implant (called SDI) system for in situ ambulatory PBM therapy, augmenting the immunity of gingival cells against potential peri-implant diseases without patient dependency (Figure 1a). Our SDI system is essentially a counterpart of the existing conventional dental implant but enables energy harvesting and light delivery using a piezoelectric

dental crown and embedded light emitting diodes (LEDs). Oral mechanical motions, such as chewing or brushing, strike SDI to cause the electrical energy generation, which is accumulated in temporary energy storage (a capacitor in our case) for irradiating embedded LEDs. Such active and localized light delivery significantly enhances PBM therapy due to consistent light delivery at extreme proximity to the peri-implant tissues. SDI also provides a high degree of spatial and temporal control of light delivery not achievable through the distant and externally delivered modalities. Importantly, SDI provides adequate mechanical strength as a dental crown. We experimentally investigate the efficacy of SDI-mediate PBM therapy using human gingival keratinocyte (HGKs) cells treated with *P. aeruginosa* LPS as a model stimulant.

2. Results

2.1. Principle of Human Oral Motion-Powered Smart Dental Implant (SDI)

To realize our SDI system and meet the clinical feasibility, we employed a screw-retained crown design which is one of the clinical standards.[21] It consisted of an implant abutment, a dental crown, an associated circuitry, micro LEDs, and a securing screw (Figure 1b,c). Notably, a key component of SDI was a dental crown that is functionalized (i.e., piezoelectric) for energy harvesting from dynamic human oral motions, such as chewing or brushing. In this study, we utilized barium titanate nanoparticles (BTNPs) as a piezoelectric material, which is a lead-free ferroelectric nanoparticle and suitable for biomedical applications.[23] The crown was composed of two-phase composite (Figure 1c): the dispersion of piezoelectric nanoparticles (0–3 composite; i.e., 0-dimension BTNPs embedded in 3-dimensions matrix) and traditional dental material attributes (1–3 composite; i.e., 1-dimension dental resin pillar embedded in 3-dimensions BTNPs-based composite). We chose the two-phase composite because the 0–1 composite offers the piezoelectric nanoparticles to afflict more directly with oral biomechanics for efficient energy harvesting,[22] and the 1–3 composite by the traditional dental material provides adequate mechanical strength under the mechanical stresses due to these oral motions[23] (Figure 1c). Additionally, we created the piezoelectric dental crown by implementing a paste extrusion 3D printing technique that enables the customized production of a patient-specific design, accommodating the patient's unique anatomy (see Materials and Methods for detailed fabrication process).[24]

Figure 1d shows scanning electron microscopy (SEM) images of BTNPs colloidal suspension and Figure 1e shows the surface morphology of postprocessed 3D printed BTNPs-fused dental crown. As seen, the postprocess (i.e., sintering) transformed scarcely connected BTNPs into a single bulk piezoelectric material. The Raman spectroscopy also confirms the piezoelectricity (Figure 1f). A sharp peak at 306 cm^{-1} indicates the signature of the tetragonal structure of barium titanate.[25] Element analysis of the SDI also confirmed the intact BTNPs after the fabrication process (Figure S1, Supporting Information). Figure 1g shows a prototype of SDI. An optical property of BTNPs (white color) was also suitable for dental material since it provides the balance between opacity and translucency the SDI to blend in with the existing teeth.

Another important component of the proposed SDI was the power management circuit that enables energy harvesting (Figure 1h).[26] We designed two different circuits for continuous wave (CW) and pulsed wave (PW) as these waveforms could enable unique PBM efficacies[27] (see also Effect of SDI-mediated LED irradiance on HGKs results). For the CW, we employed a low-loss full-wave bridge rectifier and a storage capacitor (e.g., supercapacitor) that converts the AC electrical energy into a DC electrical output. The PW was generated by using a single Schottky diode and a capacitor. A miniaturized circuit was fabricated and placed between the dental crown and an abutment (see Materials and Methods for electronics design and fabrication). Note that the bottom of a dental crown was designed to have a space for the circuit, which also allows for substantial connection to micro LEDs that were placed around the corners of the dental crown.

2.2. Energy Harvesting of Chewing and Brushing Motions

The energy harvesting performance of the SDI was evaluated using dynamic human oral motion models of chewing and toothbrushing. The electrical voltages were measured when the SDI is stimulated by chewing motion using a force application machine, which is capable of simulating antagonist strikes in accordance with controlled parameters (**Figure 2**a). To examine the efficiency of mechanical to electrical conversion, the SDI was tested without a circuit first. Figure 2b shows a representative example of the electrical voltage outputs from an SDI under chewing motion (the applied force was ≈90 N at a frequency of 5 Hz). The output showed three different regimes: a positive voltage during compression, a negative voltage during decompression, and followed by an idling trend between two different directions of forces. As an indenter initiated to compress the SDI, the electrical energy begins to increase proportionally to the applied force. At the onset of maximum compression (i.e., maximum load), the subsequent decompression surged in the polarity of voltage generation as the direction of the applied force was reversed, thus explaining the negative voltages. As an indenter returns to the base position and was lifted from the SDI, the voltage output also returned to the idle point until the next cycles start. The empirical piezoelectricity was measured to be 202 (±10.87) pC N^{-1}. The electrical voltage output was then managed via a pair of a diode and a capacitor, which converted the sinusoidal voltage outputs into a pulse wave (PW) outputs, as seen in Figure 2c. The PW output deriving LEDs in frequency mode could be more beneficial for PBM therapy (see Effect of SDI-mediated LED irradiance on HGKs results). While the frequency was determined by the oral motions, it could also be adjusted to continuous wave (CW) by implementing a rectifier circuit with a large capacitor (we used 47 μF or above to compensate for the low frequency) (Figure S2, Supporting Information). Figure 2d shows a comprehensive result of average voltage outputs of the SDI under soft food chewing motions that ranges from 30 to 100 N ($f = 5$ Hz).[28,29] The average voltage outputs were measured to be 0.4 V (±2.6 mV) to 1.3 V (±2.8 mV) as a function of applied chewing force ($V = 0.014F + 0.058$; $R^2 = 0.97$; where V is voltage and F is applied force).

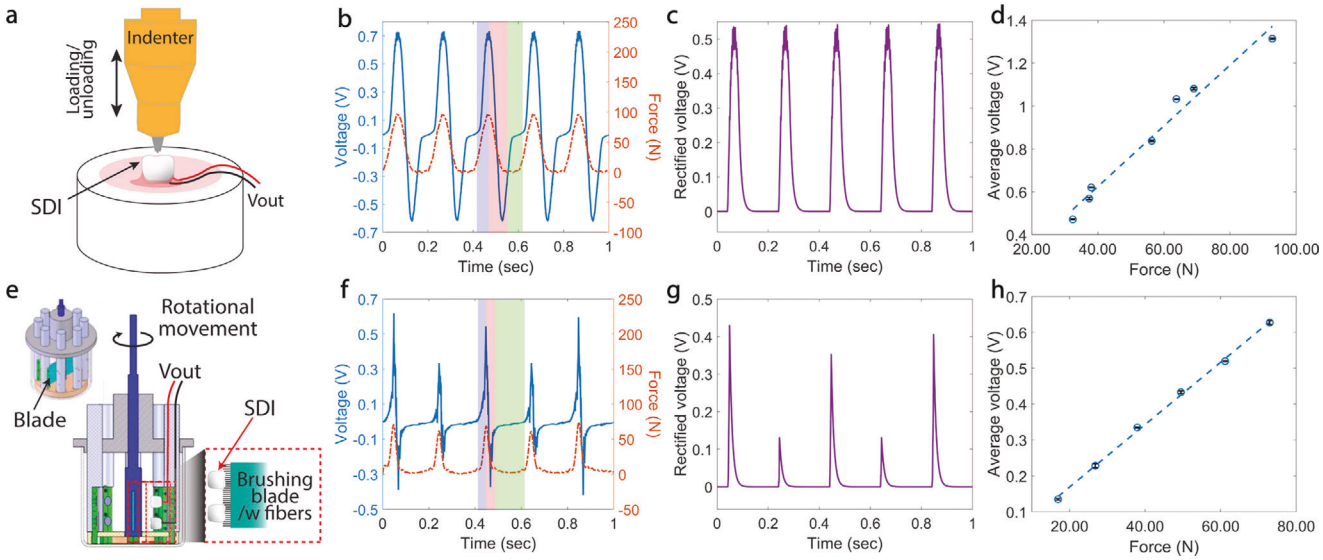

Figure 2. Generation of electrical power by mimicked human oral motions. a) The SDI under a chewing machine. b) Voltage outputs without a circuit during chewing motion: the response of SDI follows compression (blue shade), decompression (red shade), followed by an idling period (green shade). c) Converted PW using an integrated circuit, d) a comprehensive average voltage output as a function of applied force ($V = 0.014F + 0.058$; $R^2 = 0.97$). e) The SDI under a brushing machine. Adapted from "Analysis of the mechanical stability and surface detachment of mature Streptococcus mutans biofilms by applying a range of external shear forces," by Hwang et al., 2014, Biofouling: The Journal of Bioadhesion and Biofilm Research, 30(9), p. 1081 [30]. Copyright 2014 by Taylor & Francis. Adapted with permission. f) voltage outputs without a circuit during brushing: sweeping-in (blue), sweeping-out (red shade) has significantly shorter time duration, and idling period (green shade) is exceptionally longer than that in chewing motion. h) A comprehensive voltage output as a function of applied force ($V = 0.009F - 0.005$; $R^2 = 0.99$). Error bars represent standard deviation; At least three independent SDI prototypes were tested.

Figure 2e shows a brushing motion that is applied to the SDI using a custom-made shear force application machine (Figure 2e).[30] We observed similar voltage outputs to the one from the chewing machine (Figure 2f). Without a circuit, the voltage output induced by a brushing motion also had three regimes, a positive voltage due to brush fibers start sweeping in, a negative voltage as brush fibers finish sweeping and slowly lift off from the SDI, and an idle period. However, the time duration of rising and declining voltages was about half of the chewing motion (20 ms vs 40 ms). It was attributed to the force application direction respect to the poling direction of the SDI. During the fabrication, the SDI was poled in d_{33} direction (i.e., longitudinal). The chewing motion would be in the same direction as the poling, which is the preferred direction for energy harvesting.[22,26,31] In contrast, the brushing motion was perpendicular to the poling direction, d_{31} (i.e., lateral direction), whose piezoelectric constant relating the open-circuit voltage to the input mechanical stress is about half of the primary poling direction (measured to be 113 (±4.08) pC N^{-1}). As such, the converted PW exhibited varying voltage amplitude (Figure 2g). Despite half of the piezoelectric constant, the dental crown under brushing motion generated a comparable voltage output to the chewing motion: 0.7 V (±5.4 mV) vs 1.0 V (±2.8 mV) (Figure 2h). The average outputs of the SDIs ($n = 3$) were linearly proportional to applied forces as shown in Figure 2h ($V = 0.009F - 0.005$; $R^2 = 0.99$). This was due to the symmetrical nature of geometry (i.e., low aspect ratio) of the SDI that affected a large portion of a dental crown to deform in the longitudinal force even under the lateral brushing motion (the Poisson ratio compensates for the difference in d_{33} and d_{31} constants).[32]

2.3. Effects of SDI-Mediated LED Irradiances on Primary Human Gingival Keratinocytes (HGKs) Against Bacterial Inflammation

Figure 3a illustrates an experimental setup for light irradiance measurements as well as in vitro PBM therapy study, which connects the SDI under chewing or brushing machine and electronics, i.e., rectifier and a micro-LED. The results of energy harvesting from chewing and brushing motions indicated a low-power LED could be sufficiently powered (see Supplementary Information for a video clip for brushing motion demonstration). In this study, we used a single LED per well to quantify the baseline effects of light intensity to the primary human gingival keratinocytes (HGKs) in near-contact mode. Note that multiple LEDs can also be powered with the SDI under chewing or brushing motion by connecting them in a parallel configuration. We determined the electrical voltage to be 1.3 V for the red LED under chewing motion (70 N) or brushing motion (100 N). The corresponded light irradiance was measured to be 0.3 mW cm^{-2}. For the identical light irradiance, near-infrared LED required 0.8 V, which could be derived from 60 N of chewing motion or 90 N of brushing motion. All light measurement were done by a silicon photodiode in a black box (see Methods and Materials for light measurement procedure). Additionally, we performed SDI-mediated PBM therapy using pulse wave (PW) and continuous wave (CW) because our previous report on the near-contact PBM therapy revealed that the PW light therapy can be more effective than CW light therapy in some biological settings.[27] Figure 3b shows the average light irradiance from the SDI prototypes according to various PW frequencies. The average light irradiance increased in the higher frequency since a capacitor was more

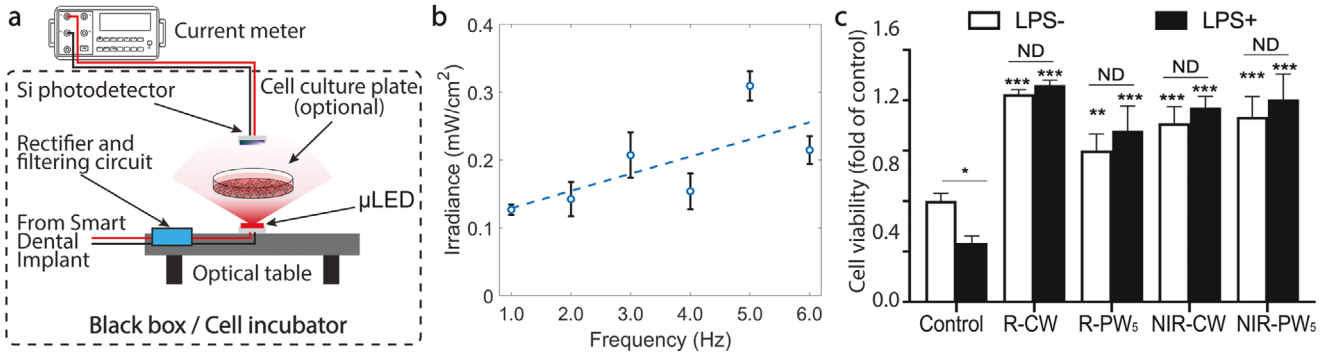

Figure 3. Cell viability test using SDI system. a) Experimental setup that separates the SDI and a LED (or cell culture plate). b) Light irradiance of one LED derived by a single SDI as a function of frequency. c) Normalized viability of HGKs with or without LPS/PBM. Error bars represent standard deviation; At least three independent experiments were performed; Asterisks indicate statistically significant changes: * ($p < 0.05$), ** ($p < 0.01$), *** ($p < 0.001$). NS indicates not significant.

frequently charged, enhancing the energy harvesting efficiency.[26] We determined the frequency of PW to be 5 Hz by adjusting the motion frequency of our oral biomechanics machine.

Next, we examined how efficiently the SDI-mediated PBM therapy can improve the viability of HGKs from bacterial invasion. In this experiment, we separated the biological study platform and the oral motion models because cultured cell and optical measurements are subject to vibrational stimulus. The output of SDI under the chewing or brushing machine (denoted as "V_{out}" in Figure 3a) was routed to an optical table with an LED and a cell plate on the surface while removing any vibrational noise (LED is placed right under the cell plate) as seen in Figure 3a. Following our established in vitro model to stimulate host cells and induce inflammation,[27] we exposed HGKs to bacterial lipopolysaccharides (LPS), which is the major virulent component of the outer membrane of Gram-negative bacteria (see Materials and Methods section for in vitro model).[33] We investigated the efficacy of our system using two experimental scenarios: 1) total energy density of 4 mJ cm^{-2} of R or NIR exposure according to 90 min of the SDI operation via chewing or brushing motions, assuming it as a total activity of daily human oral motions; 2) 10 μg mL^{-1} of LPS exposure to initiate cell inflammation without severe cell death, mimicking initial stage of bacterial infection of host cells. Note that our previous studies revealed that blue and green irradiances substantially lowered the cell viability; thus, blue and green were excluded from this study.[27] Similar to our previous study, LPS exposure to HGKs induced cell inflammation, reducing its viability by ≈20% ($p < 0.05$). In contrast, all irradiation conditions were able to fully recover the viability of HGKs against LPS stimulus. Particularly, these PBM therapies significantly increased the viability of inflamed HGKs at least 45%, up to 75% (vs control with LPS; $p < 0.001$; Figure 3c). Indeed, this remarkable improvement of cell viability exhibited 30–40% higher viability, even compared with non-inflamed HGKs ($p < 0.01$). It is noteworthy that different conditions induced different levels of treatment efficacies (the highest efficacy of 75% from R-CW or NIR-PW vs control with LPS), indicating that specific wavelength or frequency may stimulate chromophore in HGKs in a different way.

2.4. Mechanical Strength of Smart Dental Implant

The SDI system needs to have sufficient mechanical strength to withstand large chewing forces as crowns are frequently exposed to those motions, particularly in the molar region (the maximum chewing force can go up to 900 N).[34] Therefore, we experimentally validated the mechanical strength by measuring the flexural strength (FS) and flexural modulus (FM) of the mixed-mode dental composite that is used in the SDI. We used a three-point flexural test, which is a recommended method by the International Organization for Standardization (ISO) protocols that classifies dental crown materials and specifies their requirements (ISO 4049) (See Materials and Methods section for mechanical strength testing procedure).[35] Table 1 summarizes a comparison of the mechanical strength of our SDI to other materials. The dental composite used in the SDI showed FS of 50 MPa and FM of 6630 MPa, which are comparable to the mechanical strengths of dental resins reported elsewhere (FS: 65–130 MPa, FM: 2000–7500 MPa).[36–39] It indicated that our engineered dental crown could reasonably endure the impact force (flexural strength) while causing lower deflection (flexural modulus). In addition, we performed mathematical modeling of our molar design using a finite element analysis (FEA) simulation method that has been widely used to evaluate mechanical performance, thereby complying with FDA guidelines.[40] The data also confirmed that sufficient mechanical properties could be obtained and there would be free of structural defects across the 3D printed customized BTNPs-infused dental crown (Figure S3, Supporting Information).

3. Discussion

The development of an advanced dental implant system equipped with enhanced biological activity may effectively modulate the innate immunity of epithelial cells against bacterial invasion, thereby preventing peri-implant diseases. Therefore, we implemented the in situ photo-stimulation system by using a seamless piezoelectric dental implant platform. The proposed SDI system enables near-contact light delivery of two different

Table 1. Comparison of mechanical strength (flexural strength and flexural modulus).

Ref	Year	Material	Standard	FS [MPa]	FM [MPa]
This work	2020	BTNPs-infused 0–3 composite/w 3D printable dental resin 1–3 composite	ISO 4049	50 (12.9)	6630 (1100)
This work	2020	3D printable dental resin (control)	ISO 4049	90 (8.0)	3290 (590)
[49]	2016	Human dental crown	ISO 4049	114–210	–
[36]	2018	3D printable dental resin	ISO 4049	65–90	1700–2700
[37]	2018	Functionalized dental resin with nanodiamond	ISO 4049	80–110	2000–2800
[38]	2016	Enforced dental resin composite with various fillers	ISO 4049	83–161	3700–16 000
[39]	2015	Dental resin composite with silica nanostructure	ISO 4049	82–120	4000–8100

wavelengths (R or NIW) up to 4 mJ cm^{-2} energy density (Figure 2) with two operation modes, CW or PW (Figure 3). A new class of PBM therapy using the SDI may significantly increase clinical feasibility as the current light delivery method, such as a LED probe or a fiber optic, typically needs high power or a skilled clinician to interface the junctional epithelium or tissue adjacent to the implant abutment. The near-contact light delivery requires the low power to operate the LED that induces significant biological effects, thereby eliminating a cooling system to reduce heat from electronics. Our SDI system also demonstrated adequate mechanical strength that can resist external forces and stresses generated by daily oral activities, which meets with the clinical requirements.

Given the human-motion derived electrical properties of the SDI in this study, we found that either R-CW or NIR-PW irradiance can successfully promote cell proliferation under inflammatory conditions induced by LPS. In our previous study and other reports, the efficacy of PBM therapy can be varied by wavelength, energy density, irradiation time, treatment regime, operation mode (continuous waves or pulsed waves) as well as the type of cells.[27] The general consensus is that the high wavelength (e.g., red or near-infrared) improves the cell viability, while mid wavelength (e.g., green) has no significant impact regardless of energy density and the low wavelength (e.g., blue) rather reduces the cell viability.[19,27] Indeed, blue light therapy is a clinically accepted approach to kill a pathogen, such as *Propionibacterium acnes* infections.[41] Since NIR irradiation exhibited outstanding efficacy of protecting cell viability and recovering from inflammation, it may be interesting to test mixed wavelengths (e.g., blue/red or blue/near-infrared) to improve the efficacy of PBM therapy that may result in killing pathogenic bacteria without affecting the viability of host. The light intensity and operation mode are also important PBM 'dose' as the excessive energy can cause negative effects on cell viability (i.e., biphasic effect). In this study, we designed our SDI to deliver an energy level of 4 mJ cm^{-2} since we encountered the biphasic effect at 4.5 mJ cm^{-2} in our previous study.[27] Therefore, individual studies may be required to determine optimal PBM dose that is dependent on the cellular energy status (i.e., ATP level).[42,43]

Although we comprehensively demonstrated that our SDI system could be powered by human oral motion and generate sufficient energy to prevent potential peri-implant disease, it is noteworthy that the performance was tested under ideal conditions such as continuous oral motion with adequate frequencies. Therefore, a transistor switch can be added in the circuitry to store the energy (when oral motions are applied) and release stored electrical power at a later time (when sufficient energy to power LEDs is accumulated). In addition, secured packaging of the SDI will be critical for long-term reliability. While the current packaging method using parylene coating (conformal moisture and dielectric barrier) was sufficient,[44] reinforced sealing of the embedded all electronics inside of the crown may be required to avoid any mechanical contact with the oral environment. Furthermore, embedding multiple LEDs at the bottom of the crown will benefit the efficacy of SDI-mediated PBM therapy. It is to ensure the complete coverage of surrounding junctional gingival tissues where the peri-implant disease is commonly found. Also, the results on the mechanical strength of our SDI may not be significant compared to commercially available human dental crowns due to the use of dental resin. Structural improvement by introducing emerging dental material, such as zirconia, may be worth investigating in the future.

4. Conclusion

In summary, we presented an ambulatory PBM therapy modality by performing an SDI that systematically integrates energy harvesting and near-contact light delivering techniques in the form of a dental implant. The results clearly demonstrate that the SDI could convert human oral motions into controllable in situ light irradiance. In turn, we confirmed the light irradiance of the SDI could provide effective PBM therapy in the HGKs-LPS model using two effective wavelengths and two operation modes. Most significantly, to our best knowledge, the present work is the first demonstration of energy harvesting of oral biomechanics using a dental implant platform and its translational therapeutic application to ambulatory in situ PBM therapy. Provided the importance of the peri-implant disease and the feasibility of the proposed work, we look forward to the further development of the SDI, especially for the preclinical efficacy study using animal models. Therefore, improving mechanical strength by exploring other emerging dental materials, such as zirconia, will be necessary for future study. Successful completion of this translational research will lead to a highly advanced multi-functional implant system to prevent peri-implant diseases and reduce the risk of implant failure. Furthermore, this therapeutic strategy could be applied to other implant systems susceptible to constant exposure to bacterial burdens, causing adjacent host inflammation in the human body.

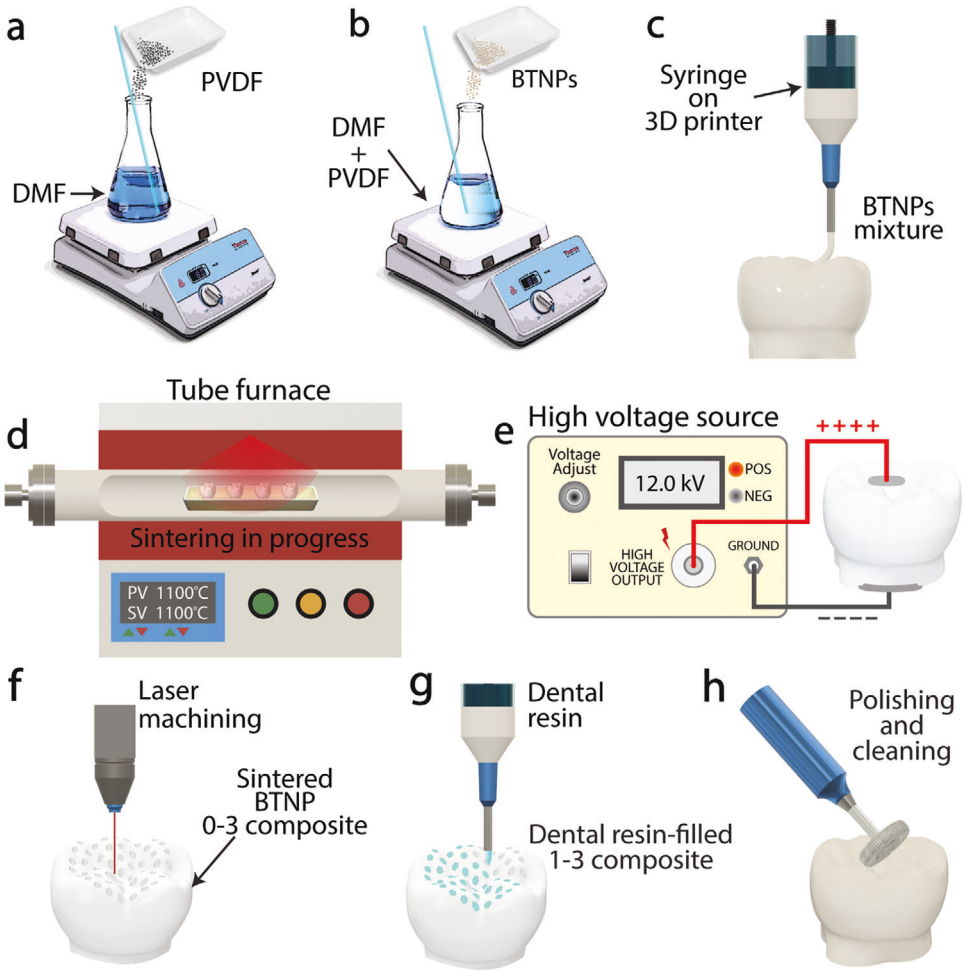

Figure 4. Fabrication procedure of SDI: a) preparing binding solution by PVDF/DFM, b) adding BTNPs for BTNPs colloidal suspension, c) loading into a syringe of the 3D printer, d) postprocessing of debinding and sintering. e) poling the postprocessed 3D printed dental crown, f) laser machining to introduce trenches to form 1–3 composite, g) filling the trenches with dental resin, and h) polishing and cleaning.

5. Experimental Section

Smart Dental Implant Fabrication: The BTNPs colloid suspension was prepared as the following. The base binder solution was first prepared by mixing polyvinyl fluoride (PVDF; Sigma Aldrich) in N,N-dimethylformamide (DMF; Sigma Aldrich) by a weight ratio of 1:8.8 at 80 °C for 15 min (**Figure 4**a).[45] The BTNPs (400 nm, US Research Nanomaterials) was slowly added into the binder solution while continuously stirring by hand until it reached a high-volume concentration (Figure 4b). The empirical result found that the binder solution could take up to 332 wt% of BTNPs. The BTNPs suspensions were then loaded to a syringe (10 mL) with 600 µm nozzle, followed by installing to a paste extrusion 3D printer (Tissue Scribe, Culture3Ds) (Figure 4c). The printing speed was adjusted to 1 mm s^{-1} with a *z*-resolution of 400 µm. The printed SDI was then dried at 120 °C for 2 h to evaporate DMF, completing the green material. The postprocessing of debinding and sintering were subsequently performed using a tubing furnace (GSL-1500X, MTI Corporation) (Figure 4d).[22,45] The temperature profile for debinding was at 650 °C for 1 h (ramp rate = 5°C min^{-1}), followed by sintering at 1400 °C for 3 h (ramp rate = 5 °C min^{-1}) (Figure S4, Supporting Information). After the postprocess, the SDI was poled to align randomly oriented ferroelectric domains (Figure 4e). For that, the SDI received temporary electrodes at top and bottom by applying silver epoxy (8331, MG Chemicals), which was applied and dried at 60 °C for 1 h. The SDI was then placed on the custom-made poling stage that has a copper bottom plate and a spring-loaded needle electrode from the top. The poling stage was also equipped with a built-in heating element in a silicone oil bath. Using the poling stage and a high voltage source (230-30R, Spellman), a uniform electric field of 1 kV mm^{-1} was applied across the SDI while the temperature of the silicone oil bath was set below the Curie temperature for BTNPs (80 °C). The total poling time was 4 h. The SDI was then modified using a laser machine (VLS6.60, Universal Laser Systems) to create honeycomb-inspired trenches for 1–3 composite configuration, which reinforces the mechanical strength (Figure 4f). The trench size was 1 mm in diameter. The trenches were filled with ultraviolet (UV) light curable dental crown resin (C&B Micro Filled Hybrid, NextDent). Note that other dental material, such as dental resin, metal, or ceramic (e.g., zirconia) can be used. Prior to filling the trenches, the dental resin was stirred overnight on a rotational mixer platform. The sidewall of the dental crown was also enforced by coating with the dental resin. After filling, the SDI was degassed for an hour, followed by UV light curing (100402-400, IntelliSpense). Lastly, the fabricated piezoelectric dental crown was sanded and polished for the final touch (Figure 4h). As the filling process often created residues on the surface, the dental crown could be further polished and adjusted to the desired shape as necessary.

Fabrication of Electronics: Miniaturized electronics to be housed in a small space were also fabricated at the bottom of SDI. To facilitate the miniaturization of electronics, surface-mount components were used on a printed circuit board (PCB) that was manufactured via a traditional

lithography method. The circuit layout was designed using a schematic software (Eagle CAD), which was transferred to a copper-laminated PCB board (FR4, MG Chemicals) via a shadow mask technique. After etching the copper defined by the shadow mask, all components were substantially assembled to the PCB. Multiple LEDs could also be installed at the bottom of the SDI in the prepared grooves. The choices of all components were mm-scale, which fit everything inside of the small PCB ($4 \times 4 \times 1$ mm^3). The low-power LEDs with two distinctive wavelengths were selected: 615 nm for R (APTD1608, Kingbright), and 880 nm for NIR (SML-P11x, Rohm), a supercapacitor (CPH3225A, Seiko), Schottky diode array (CMRSH-4DO, Central Corp), and resistors (CRCW0201, Vishay). Upon the assembly of all discrete components, the circuit was coated with 5 µm thick of Parylene-C (Specialty Coatings) for electrical passivation and protection. Parylene is widely used encapsulation material for electronics due to its pinhole-free conformal coating and excellent moisture and dielectric barrier.[44] Lastly, the PCB was assembled to the SDI using a dental adhesive (Panavia, Kuraray Medical Inc.), then a retaining screw mounts the SDI assembly onto the implant post securely.

Light Measurement: The light measurement was done on an optical table. An LED was connected to the SDI via 10 cm-long polyimide coated copper wires and was securely mounted on the floor of the optical table. While the SDI was stimulated under the oral motions, light irradiance was measured using a silicon photodiode (FDS1010, Thorlabs) from the top. The distance between the LED and the photodiode was ≈5 mm. The photodiode output was then measured using a precision current meter (2400, Keithley). Note that all measurements were done inside of the black box to eliminate the ambient light. The light energy density was calculated based on the measured irradiance and frequency. The light energy density of PW due to chewing or brushing motions was measured to be 0.77 µJ cm^{-2} s^{-1} at 5 Hz, which in turn 4.1 mJ cm^{-2} for 90 min of exposure.

Dental Biomechanics: Chewing and Brushing Machines: Two different human oral motions were modeled: chewing and brushing. For the chewing model, an electromechanical universal test machine (311R, TestResources, Inc.) was programmed. It was capable of simulating antagonist strikes in accordance with controlled parameters by adjusting the traverse paths of the axles and the speeds. A series of complete chewing cycles were executed onto the distobuccal cusp of SDI. The counterweight was also varied, which loads the antagonists and generates contact pressure during the abrasive motion. Based on the existing literature, the soft food chewing motion parameters were employed[29,46]: speed = 20–40 mm s^{-1}, force = 0–200 N, and frequency = 1–5 Hz.

For the brushing model, the custom-design rotational apparatus was built. The rotation was induced by a motor (BDC3030, Caframo Limited) that holds a central steel rod with a square blade at the bottom. On the blade, two toothbrush heads were mounted at each end. The central rod was then placed on top of a circular platform, which also holds multiple plastic rods on its edge; thus, the brush heads could sweep the SDI mounted on a plastic rod as on the central rod rotates. On the plastic rods, a designated space was introduced to mount the SDI. The filaments of the brush overlapped ≈5 mm of the SDI. Based on the existing literature, the brushing motion parameters were employed[47,48]: speed = 2 mm s^{-1}, normal force = 12 N (assuming 600 filaments sweep the SDI on each stroke and normal force due to a single filament was ≈20 mN[47]), shear force = 15–70 N, and frequency = 1–5 Hz.

Scanning Electron Microscopy: The surface morphology of SDI was characterized using Field Emission Scanning Electron Microscopy (Quanta, FEG 450). Elemental analysis of SDI was performed using Energy-dispersive X-ray spectroscopy (Quanta, FEG 450). The SEM working distance was 9.64 µm (Figure 1d) and 9.77 µm (Figure 1e), respectively. The magnification was 2500× for Figure 1d and 5000× for Figure 1e. The field height × width was 82.9 × 55.3 µm, with a resolution of (1536 × 1024 pixel^2).

Measurement of Flexural Strength and Flexural Modulus: An electromechanical universal test machine (311R, TestResources Inc.) was used with ISO 4049 (Dentistry—Polymer-based restorative materials)-specific test fixtures for the comprehensive mechanical evaluation[35] (**Figure 5**). A three-points flexural bend fixture was used. A total of ten beam structures ($25 \times 2 \times 2$ mm^3) were prepared based on the same mixed-mode composite configuration, BTNPs-infused 0–3 composite with 1–3 composite enforcement. The same beam structure was also prepared with dental resin for the comparison. Force and deformation were substantially measured. The FS and FM were then calculated using the following equations

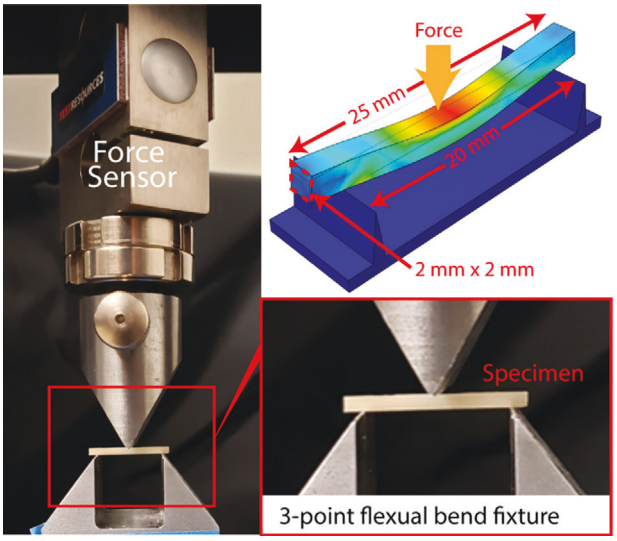

Figure 5. ISO 4049-specific three-point flexural bend fixture for mechanical strength evaluation.

$$\mathrm{FS} = \frac{3FL}{2bh^2} \quad (1)$$

$$\mathrm{FM} = \frac{FL^3}{4dbh^3} \quad (2)$$

where b = beam width (mm), h = beam depth (mm), F = load at a given point on the load deflection curve (N), L = support span (mm), and d = corresponding deflection at F (mm).

Cell Culture and Cell Viability Assay: Primary human Gingival Keratinocytes (HGKs) cells were kindly provided by the laboratory of Dr. Dana T. Graves at the University of Pennsylvania and cultured in Kaighn's Modification of Ham's F-12 Medium (F-12K Medium; 10-025-CV, Corning, Costar, NY) containing 10% v/v fetal bovine serum (FBS; 16140071, Gibco, Belgium) and 100 U mL^{-1} of Antibiotic-Antimycotic (15240096, Gibco, Belgium) at 37°C in a humid atmosphere of 5% CO_2. Initially, HGKs cells were seeded at 1×10^4 cells per well in 24-well plates and grown for 24 h at 37 °C. After 24 h of incubation, cells were washed with 1× PBS and incubated in medium without FBS for an additional 48 h after relevant treatments (LED irradiation and/or LPS treatment). Cell viability was determined at 0, 24, and 48 h using MTT (3-(4,5-Dimethylthiazol-2-yl)-2,5-diphenyltetrazolium bromide) (Cell proliferation kit I, Roche, Germany) as described elsewhere.[51] Briefly, 50 µL of the MTT labeling reagent (final concentration of 0.5 mg mL^{-1}) was added to each well. Then, the cells were incubated in a CO_2 incubator at 37 °C for 4 h. 500 µL of the Solubilization buffer (10% SDS in 0.01 M HCl) was added and the plate was allowed to stand overnight in the incubator to solubilize the formazan crystals. The optical density (OD) values of samples were then measured at a wavelength of 570 nm with a microplate reader (BioTek, Winooski, VT). OD values of the treatment groups were always normalized to that of the untreated control group.

Cell Inflammation by Bacterial LPS: To investigate the cell response to bacterially induced inflammation, the cells to were exposed lipopolysaccharide (LPS; L9143, Sigma, St. Louis, MO). First, the optimal concentration of LPS was determined for inflammation induction by adding various concentrations of LPS (0–100 µg mL^{-1}). After A549 cells were grown for

24 h, the cells were washed and the culture medium was replaced with fresh media (0% FBS). Then, LPS was added and the cells were subsequently incubated for an additional 24 h. With a predetermined optimal concentration of LPS (0–20 μg mL^{-1}), the cells were also pretreated with the STI before LPS exposure, as described in the previous section on PBM therapy, and the cells were subsequently incubated for an additional 24 h. Then, the viability of cells was evaluated using the MTT assay (see Cell culture and cell viability assay for detail).

Statistical Analysis: At least three independent experiments were performed for each experiment mentioned above. The results from independent experiments were expressed as mean ± standard deviation. Statistical analysis was carried out using GraphPad Prism 8 software via unpaired t-tests. The level of significance was set at 5%.

Supporting Information

Supporting Information is available from the Wiley Online Library or from the author.

Acknowledgements

M.P. and S.I. contributed equally to this work. The authors would like to thank Dr. Fei Ran and his students, Zhu Long, Weixiao Gaio, Jiaxin Xi (Temple University) for providing an access to a tube furnace, Dr. Mehdi Moradllo and Zeinab Bahmanzadeh for assistance in obtaining the initial thermal gravity analysis of BTNPs. This work was partially supported by Temple University start-up funds (A.K.) and University of Pennsylvania start-up (G.H.).

Conflict of Interest

The authors declare no conflict of interest.

Keywords

dental implants, energy harvesting, peri-implant disease, photobiomodulation, piezoelectric implants

Received: April 21, 2020
Revised: May 21, 2020
Published online:

[1] H. W. Elani, J. R. Starr, J. D. Da Silva, G. O. Gallucci, *J. Dent. Res.* **2018**, *97*, 1424.
[2] A. Johannsen, A. Westergren, G. Johannsen, *J. Clin. Periodontol.* **2012**, *39*, 681.
[3] H.-J. Nickenig, M. Wichmann, S. K. Andreas, S. Eitner, *J. Cranio-Maxillofacial Surg.* **2008**, *36*, 477.
[4] G. Charalampakis, Å. Leonhardt, P. Rabe, G. Dahlén, *Clin. Oral Implants Res.* **2012**, *23*, 1045.
[5] P. Rosen, et al., *J. Periodontol.* **2013**, *84*, 436.
[6] S. Sakka, K. Baroudi, M. Z. Nassani, *J. Investigat. Clin. Dent.* **2012**, *3*, 258.
[7] M. A. Atieh, N. H. Alsabeeha, C. M. Faggion, W. J. Duncan, *J. Periodontol.* **2013**, *84*, 1586.
[8] P. Papaspyridakos, C.-J. Chen, S.-K. Chuang, H.-P. Weber, G. O. Gallucci, *Int. J. Oral Maxillofac. Implants* **2012**, *27*, 102.
[9] B. E. Pjetursson, K. Tan, N. P. Lang, U. Brägger, M. Egger, M. Zwahlen, *Clin. Oral Implants Res.* **2004**, *15*, 625.
[10] D. M. Daubert, B. F. Weinstein, S. Bordin, B. G. Leroux, T. F. Flemmig, *J. Periodontol.* **2015**, *86*, 337.
[11] N. U. Zitzmann, T. Berglundh, *J. Clin. Periodontol.* **2008**, *35*, 286.
[12] H. Ikeda, M. Shiraiwa, T. Yamaza, M. Yoshinari, M. A. Kido, Y. Ayukawa, T. Inoue, K. Koyano, T. Tanaka, *Clin. Oral Implants Res.* **2002**, *13*, 243.
[13] Y. Wang, Y. Zhang, R. J. Miron, *Clin. Implant Dent. Relat. Res.* **2016**, *18*, 618.
[14] N. Claffey, E. Clarke, I. Polyzois, S. Renvert, *J. Clin. Periodontol.* **2008**, *35*, 316.
[15] E. Figuero, F. Graziani, I. Sanz, D. Herrera, M. Sanz, *Periodontol. 2000* **2014**, *66*, 255.
[16] S. Renvert, A.-M. Roos-Jansåker, N. Claffey, *J. Clin. Periodontol.* **2008**, *35*, 305.
[17] X. Ren, H. C. van der Mei, Y. Ren, H. J. Busscher, *Acta Biomater.* **2019**, *96*, 237.
[18] F. Song, H. Koo, D. Ren, *J. Dent. Res.* **2015**, *94*, 1027.
[19] J. J. Anders, R. J. Lanzafame, P. R. Arany, *Photomed. Laser Surg.* **2015**, *33*, 183.
[20] A. P. Sommer, A. L. Pinheiro, A. R. Mester, R.-P. Franke, H. T. Whelan, *Photomed. Laser Surg.* **2001**, *19*, 29.
[21] I. Sailer, S. Mühlemann, M. Zwahlen, C. H. Hämmerle, D. Schneider, *Clin. Oral Implants Res.* **2012**, *23*, 163.
[22] R. I. Mahdi, W. H. Abd. Majid, *RSC Adv.* **2016**, *6*, 81296.
[23] G. Tagliavia, M. Porfiri, N. Gupta, *Composites, Part B* **2010**, *41*, 86.
[24] A. Dawood, B. M. Marti, V. Sauret-Jackson, A. Darwood, *Br. Dent. J.* **2015**, *219*, 521.
[25] M. Acosta, N. Novak, V. Rojas, S. Patel, R. Vaish, J. Koruza, G. A. Rossetti Jr., J. Rödel, *Appl. Phys. Rev.* **2017**, *4*, 041305.
[26] *Energy Harvesting Technologies* (Eds: S. Priya, D. J. Inman), Springer, Boston, MA **2009**.
[27] H.-E. Kim, S. Islam, M. C. Park, A. Kim, G. Hwang, *Adv. Biosyst.* **2020**, *4*, 1900227.
[28] S. D. Heintze, A. Eser, D. Monreal, V. Rousson, *J. Mech. Behav. Biomed. Mater.* **2017**, *65*, 770.
[29] *Dental Biomechanics*, (Ed: A. N. Natali), Taylor & Francis, London **2003**.
[30] G. Hwang, M. I. Klein, H. Koo, *Biofouling* **2014**, *30*, 1079.
[31] E. K. Akdogan, M. Allahverdi, A. Safari, *IEEE Trans. Sonics Ultrason.* **2005**, *52*, 746.
[32] S. H. Song, A. Kim, B. Ziaie, *IEEE Trans. Biomed. Eng.* **2015**, *62*, 2717.
[33] C. V. Rosadini, J. C. Kagan, *Curr. Opin. Immunol.* **2017**, *44*, 14.
[34] R. Okada, M. Asakura, A. Ando, H. Kumano, S. Ban, T. Kawai, J. Takebe, *J. Prosthodont. Res.* **2018**, *62*, 287.
[35] International Organization for Standardization, "ISO 4049:2019 Dentistry—Polymer-based restorative materials," https://www.iso.org/standard/67596.html. Accessed date: April 1st, 2020.
[36] A. Tahayeri, M. Morgan, A. P. Fugolin, D. Bompolaki, A. Athirasala, C. S. Pfeifer, J. L. Ferracane, L. E. Bertassoni, *Dent. Mater.* **2018**, *34*, 192.
[37] W. Cao, Y. Zhang, X. Wang, Q. Li, Y. Xiao, P. Li, L. Wang, Z. Ye, X. Xing, *J. Mater. Sci.: Mater. Med.* **2018**, *29*, 162.
[38] L. D. Randolph, W. M. Palin, G. Leloup, J. G. Leprince, *Dent. Mater.* **2016**, *32*, 1586.
[39] R. Wang, M. Zhang, F. Liu, S. Bao, T. Wu, X. Jiang, Q. Zhang, M. Zhu, *Mater. Sci. Eng., C* **2015**, *50*, 266.
[40] Food and D. Administration, "Reporting of Computational Modeling Studies in Medical Device Submissions: Guidance for Industry and Food and Drug Administration Staff," **2016**.
[41] T. Dai, A. Gupta, C. K. Murray, M. S. Vrahas, G. P. Tegos, M. R. Hamblin, *Drug Resist. Updates* **2012**, *15*, 223.
[42] H. B. Kim, K. Y. Baik, P.-H. Choung, J. H. Chung, *Sci. Rep.* **2017**, *7*, 15927.

[43] G. K. Keshri, A. Gupta, A. Yadav, S. K. Sharma, S. B. Singh, *PLoS One* **2016**, *11*, 0166705.
[44] C. Hassler, R. P. von Metzen, P. Ruther, T. Stieglitz, *J. Biomed. Mater. Res., Part B* **2010**, *9999B*, NA.
[45] H. Kim, A. Renteria-Marquez, Md D. Islam, L. A. Chavez, C. A. Garcia Rosales, Md A. Ahsan, T.-L. Bill Tseng, N. D. Love, Y. Lin, *J. Am. Ceram. Soc.* **2019**, *102*, 3685.
[46] J. M. C. Po, J. A. Kieser, L. M. Gallo, A. J. Tésenyi, P. Herbison, M. Farella, *J. Dent. Res.* **2011**, *90*, 1206.
[47] F. Goldschmidtboeing, A. Doll, U. Stoerkel, S. Neiss, P. Woiase, *J. Mech. Eng.* **2014**, *60*, 449.
[48] H. R. Rawls, N. J. Mkwayi-Tulloch, M. E. Krull, *Dent. Mater.* **1990**, *6*, 111.
[49] Y. Shinno, T. Ishimoto, M. Saito, R. Uemura, M. Arino, K. Marumo, T. Nakano, M. Hayashi, *Sci. Rep.* **2016**, *6*, 19849.